J. Membrane Biol. 161, 163–171 (1998)

The Journal of
Membrane
Biology

Characterization of Calcium-activated Chloride Channels in Patches Excised from the Dendritic Knob of Mammalian Olfactory Receptor Neurons

M. Hallani[1], **J.W. Lynch**[2,3], **P.H. Barry**[1]

[1]School of Physiology and Pharmacology, University of New South Wales, Sydney, Australia, 2052
[2]Neurobiology Program, Garvan Institute of Medical Research, Darlinghurst, Sydney, NSW, Australia, 2010
[3]Department of Physiology and Pharmacology, University of Queensland, St. Lucia, QLD, Australia, 4072

Received: 16 April 1997/Revised: 3 October 1997

Abstract. We investigated the properties of calcium-activated chloride channels in inside-out membrane patches from the dendritic knobs of acutely dissociated rat olfactory receptor neurons. Patches typically contained large calcium-activated currents, with total conductances in the range 30–75 nS. The dose response curve for calcium exhibited an EC_{50} of about 26 μM. In symmetrical NaCl solutions, the current-voltage relationship reversed at 0 mV and was linear between −80 and +70 mV. When the intracellular NaCl concentration was progressively reduced from 150 to 25 m*M*, the reversal potential changed in a manner consistent with a chloride-selective conductance. Indeed, modeling these data with the Goldman-Hodgkin-Katz equation revealed a P_{Na}/P_{Cl} of 0.034. The halide permeability sequence was $P_{Cl} > P_F > P_I > P_{Br}$ indicating that permeation through the channel was dominated by ion binding sites with a high field strength. The channels were also permeable to the large organic anions, SCN^-, $acetate^-$, and $gluconate^-$, with the permeability sequence $P_{Cl} > P_{SCN} > P_{acetate} > P_{gluconate}$. Significant permeation to gluconate ions suggested that the channel pore had a minimum diameter of at least 5.8 Å.

Key words: Olfactory receptor neuron — Chemosensory transduction — Organic anion — Halide anion — Ca^{++}-activated Cl^- channel

Introduction

Vertebrate olfactory receptor neurons respond to odorant stimulation with a G protein-mediated increase in the concentration of cAMP. The primary effect of cAMP is to directly activate a cyclic nucleotide-gated (CNG) cation-selective ion channel (Reed, 1992; Dionne & Dubin, 1994). Under physiological concentrations of extracellular calcium, these channels are highly selective for calcium (Frings et al., 1995). By acting as a permeation pathway for calcium ions into the cell, CNG channels can either directly depolarize the cell (Firestein, Darrow & Shepherd, 1991) or activate a calcium-activated chloride current (Kleene, 1993; Kurahashi & Yau, 1993, 1994). This chloride current can be as large as the CNG cation current, suggesting that it plays a crucial role in the olfactory transduction process (Kurahashi & Yau, 1993, 1994). Indeed, chloride currents activated by calcium influx through CNG channels were shown to dramatically amplify the odorant-induced current, demonstrating a role for these channels in improving the signal-to-noise ratio of olfactory transduction (Lowe and Gold, 1993).

Despite their importance in the olfactory transduction process, little is known about the biophysical properties of calcium-activated chloride channels. The channels were first identified in isolated olfactory cilia from the frog by Kleene and Gesteland (1991), where it was shown that the activation of these channels by calcium was rapid and fully reversible and that they were highly selective for Cl^- over Na^+ and K^+. They further found the EC_{50} for calcium-activation was 5 μM and that the steepness of the dose-response curve suggested a cooperative calcium-dependent activation mechanism. The channels were found to be blocked by 3′,5-dichlorodiphenylamine-2-carboxylate and niflumic acid (Kleene & Gesteland, 1991; Kleene, 1993).

In this paper, we investigate the biophysical properties of calcium-activated chloride channels in inside-out patches excised from the apical membrane of rat olfac-

Correspondence to: P.H. Barry

tory receptor neurons. Patches contained surprisingly large numbers of channels, with total calcium-activated patch conductances of up to 75 nS. We describe the calcium-dependence of chloride channel activation, investigate the halide selectivity sequence and provide an estimate of the minimum pore diameter using large monovalent organic anions.

Materials and Methods

Cell Preparation

Olfactory receptor neurons from adult Wistar rats were enzymatically dissociated according to the method described by Lynch and Barry (1991). Briefly, olfactory epithelia were dissected, cut into small pieces and the cells dissociated in divalent cation-free Dulbecco's phosphate buffered saline (DPBS) containing 0.2 mg/ml of trypsin (Calbiochem, La Jolla, CA). Tissue pieces were then incubated for 27 min at 37°C. Following this, the trypsin solution was removed and replaced with 10 ml of General Mammalian Ringers (GMR) solution containing 0.1 mg of trypsin inhibitor (Calbiochem, La Jolla, CA). Following gentle trituration of the dissociated epithelia with a wide-bored pipette, 2 ml of the supernatant were pipetted into a glass-bottomed recording chamber. These cells were left to settle for 30 min before they were continually superfused with the GMR, containing (in mM): NaCl 140, KCl 5, $CaCl_2$ 2, $MgCl_2$ 1, Glucose 10 and HEPES 10 (pH 7.4 with NaOH). Olfactory receptor neurons were distinguished by their characteristic bipolar morphology. All experiments were performed at room temperature (20–22°C).

Solutions and Perfusion System

The patch pipette solution used in all experiments contained (in mM): NaCl 140, EGTA 10, NaOH 25 and HEPES 10, titrated to pH 7.4 with NaOH. The zero calcium control solution used to bathe the cytoplasmic surface of excised patches contained (in mM): NaCl 155, EGTA 2, NaOH 10 and HEPES 10, titrated to pH 7.4 with NaOH. This solution is referred to as the '0Ca' solution. In experiments where the calcium concentration was varied, the solution composition was similar to this except that EGTA was omitted, and concentrations of calcium chloride ranging between 1 μM and 1 mM were added. The deionized water used for making up the solutions was shown to have less than 0.1 μM [Ca^{2+}] and later measurements of calcium contaminants in the 155 mM NaCl and Na HEPES buffer were shown to indicate about 0.7 μM [Ca^{2+}]. These calcium measurements were made by inductively coupled plasma atomic emission spectrometry and their implications will be discussed later. In both NaCl dilution experiments and anion substitution experiments, EGTA was also omitted and calcium-activated currents were measured by subtracting responses in solutions containing no added calcium from those containing 0.2 mM calcium. In dilution experiments, the NaCl concentration was reduced from 155 to 100, 50 and 25 mM. In anion substitution experiments, all NaCl was replaced by the sodium salt of the test anion. In these bi-ionic measurements, 140 mM was used for all the test salts to be at the same concentration as the NaCl in the pipette. Halide anions (F^-, I^-, and Br^-) and organic anions (SCN^-, acetate$^-$ and gluconate$^-$) were sequentially substituted for Cl^- in these experiments.

The glass-bottomed bath chamber used in these experiments (Fig. 1*A*) consisted of two compartments connected via a canal. One chamber contained the cells which were continually superfused with GMR. Once an excised patch was formed by brief air exposure of cell-attached patches, the pipette was moved through the connecting canal into the other chamber which contained a parallel multi-jet perfusion system, which allowed the solution bathing the patch to be rapidly exchanged.

Electrophysiological Recordings

Calcium-activated chloride currents were studied in inside-out patches from the dendritic knob of isolated olfactory receptor neurons using standard patch-clamp techniques (Hamill et al., 1981). Patch pipettes were fabricated from borosilicate haematocrit tubing (Cat. No. 1601, Vitrex Modulohm, Herlev, Denmark) and had tip diameters of about 0.2 μm with access resistances of 10–15 MΩ when filled with the standard pipette solution. In all protocols used in this study, patches were held at a membrane potential of 0 mV and step voltage pulses of 180 msec duration were applied from voltages between −80 and +70 mV, in 10 mV steps. The resultant current responses were measured with an Axopatch-1D patch-clamp amplifier (Axon Instruments, Foster City, CA), filtered at 1 kHz and recorded onto an IBM compatible 486-DX2 66 MHz computer using pClamp software (V.6.0; Axon Instruments, Foster City, CA). Junction potential corrections were calculated with the Windows version of JPCalc (Barry, 1994). Although the actual reference electrode was a 155 mM NaCl salt bridge, the effective reference solution was the intermediate region of GMR between the solution jet and the reference electrode (*see* Fig. 1*A*). The dose-response curves were constructed from current amplitudes normalized (I_{norm}) with respect to the maximum current obtained at 1 mM $CaCl_2$ in the same patch. Except where indicated, all data points were averaged from 4 to 5 patches, and the error bars represent standard errors of the mean (±SEM).

Results

Calcium-dependence of the Patch Current

The first aim of this study was to establish the presence of a calcium-activated conductance in excised patches from the dendritic knob of rat olfactory receptor neurons. The method by which this was achieved is summarized in Fig. 1*B*. Patches were initially exposed to 0Ca solution and voltage steps were applied from −80 to +70 mV in 10 mV steps of 180 msec duration. However, in all figures only current responses to voltages from −60 to +60 mV in 20 mV steps are shown. As seen in Fig. 1*B*i, a significant background leakage current was observed in 0Ca solution. In the presence of 0.2 mM calcium, the patch conductance was dramatically increased (Fig. 1*B*ii). Following digital subtraction of the background leakage current, the calcium-dependent current component was isolated (Fig. 1*B*iii). Upon removal of calcium, the leakage current returned to the control level (Fig. 1*B*iv). The maximum amplitude of the calcium-activated patch conductance varied between 30 and 75 nS. The next step was to quantitate the calcium-dependence of this current. To achieve this, the following nominal range of calcium concentrations was tested on each patch: 0, 1, 10, 20, 50, 100, 200, 500 and 1000 μM (small corrections for calcium contaminants in the solutions

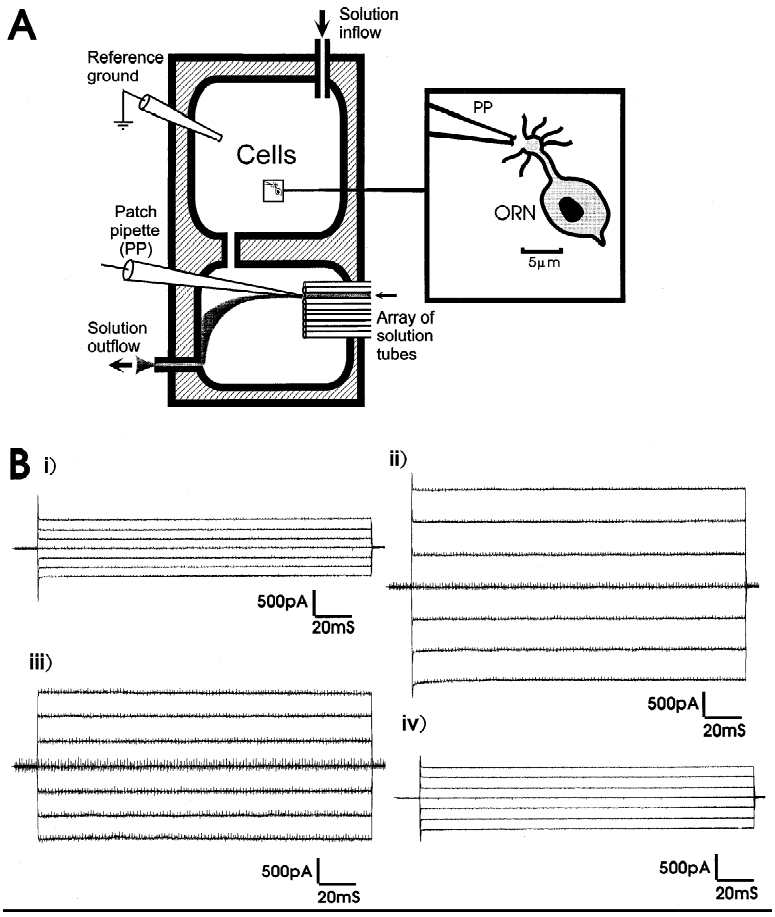

Fig. 1. (*A*). Illustration of the perfusion system. The area labeled 'cells' contained the dissociated cells. Following inside-out patch formation in this area, pipettes were moved through the canal into the adjacent chamber and placed in front of an array of tubes through which different test solutions flowed. (*B*): Examples of current recordings obtained from a single inside-out patch. Current traces in this and all subsequent figures are shown in response to voltage steps at 20-mV intervals from −60 to +60 mV. (i) Background leakage currents recorded in 0Ca solution. (ii) Total current response in 0.2 mM calcium. (iii) Current activated by 0.2 mM calcium after digital subtraction of leakage current. (iv) Background leakage current after washout of 0.2 mM calcium.

will be discussed later). Membrane patches were maintained in 0Ca solution for at least 2 min between different test calcium concentrations to minimize the effects of desensitization and chloride accumulation. Examples of currents activated by the increased calcium concentrations in one patch are shown in Fig. 2. Background leakage currents have been subtracted from all traces. Data from the patch shown in Fig. 2 were used to construct the family of current-voltage (*I-V*) relationships shown in Fig. 3*A*. A later measured contamination of about 0.7 μM $[Ca^{2+}]$ for solutions with 155 mM NaCl and Na HEPES buffer was used to correct the data values. Dose-responses from this patch and three others were averaged to produce the calcium dose-response curve shown in Fig. 3*B* and the maximum uncertainty due to the greatest limit of calcium contamination of these salts (about 4.5 μM; from the chemical company's specifications) has been allowed for by the horizontal error bars in the figure. This curve was fitted using a Hill type equation:

$$I_{\text{norm}} = C^h/[C^h + \text{EC}_{50}{}^h] \quad (1)$$

where I_{norm} is the normalized current, C is the calcium concentration and h is the Hill coefficient. The calcium concentration required for half-maximal current activation (EC_{50}) was about 26 μM, with the Hill coefficient close to 1, although with errors indicated not too much weight should be placed on this latter value. From these results, it was obvious that the activation of these currents was directly dependent on the calcium concentration. The ionic selectivity of this current was then investigated.

Chloride-dependence of the Calcium-activated Conductance

To determine the selectivity of this conductance for Cl^- over Na^+ ions, the concentration of NaCl bathing the exposed (intracellular) surface of the patch was progressively reduced from 150 mM to 100, 50 and 25 mM, while reductions in osmolarity were compensated by the addition of sucrose. Averaged results from 5 patches exposed sequentially to the four different NaCl concentrations are shown in Fig. 4. Currents were activated by 0.2 mM calcium, and the respective background leakage currents measured in 0Ca solution have been subtracted. From these *I-V* relationships, it is clear that there was a

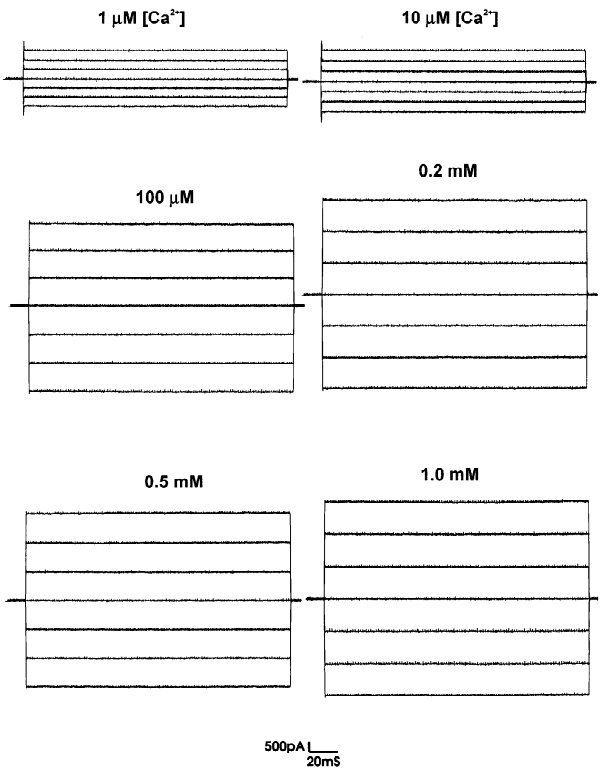

Fig. 2. Examples of currents recorded in one patch in response to increasing concentrations of calcium (for corrected estimates of calcium concentrations *see* legend to Fig. 3). Background leakage currents in the absence of calcium have been subtracted for each series of traces. Calcium-activated currents saturate near 0.2 mM calcium. The scale bars apply to all panels.

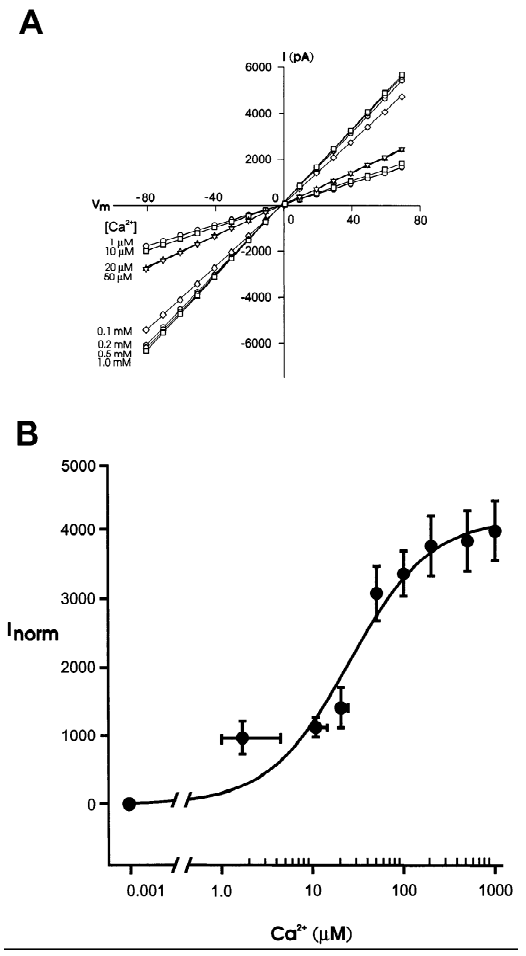

Fig. 3. Calcium dose-response curve for the calcium-activated current. (*A*): *I-V* (current-voltage) relationships at different nominal calcium concentrations from the patch displayed in Fig. 2. Saturation occurs near 0.2 mM calcium. (*B*): Dose-response curve for calcium activation of the current, with the normalized patch current (I_{norm}) plotted against the calcium concentration. 0.7 μM calcium has been added to all the nominal calcium concentrations to allow for a later measured calcium contamination from 155 mM NaCl solutions and the horizontal error bars are to allow for the greatest limit of calcium contamination of these salts (from the chemical company's specifications). The curve was fitted with a Hill type equation (Eq. 1), with an EC_{50} of about 26 μM and a Hill coefficient (*h*) close to 1. The data points were averaged from 4 patches and the vertical error bars in this and all subsequent figures represent standard errors of the mean (±SEM).

progressive attenuation in the current as the concentration of the NaCl was lowered. It is also evident that the reversal potential (E_{rev}) had progressively shifted to more negative potentials as the concentration of NaCl was reduced. The reversal potentials, measured for each NaCl concentration, were averaged and plotted against the activities of NaCl in Fig. 5. The Goldman-Hodgkin-Katz equation was then used to calculate the ratio of the permeability of sodium and the permeability of chloride (P_{Na}/P_{Cl}) in the form:

$$E_{rev} = (RT/F)\cdot\ln[(P[Na]_o + [Cl]_i)/(P[Na]_i + [Cl]_o)] \quad (2)$$

where $P = P_{Na}/P_{Cl}$, E_{rev} is the reversal potential, RT/F (with R being the gas constant, T the temperature in Kelvin and F the Faraday constant) equals 25.34 mV at 21°C, and $[Na]_o$, $[Na]_i$, $[Cl]_o$ and $[Cl]_i$ are the activities of sodium and chloride on the extracellular and intracellular membrane surfaces respectively. The values of the NaCl activities were extrapolated for each of the concentrations from tables of Robinson & Stokes (1965). Equation (2) can be rearranged to express P_{Na}/P_{Cl} in terms of E_{rev} as follows:

$$P_{Na}/P_{Cl} = (\exp(E_{rev}/25.34)\cdot[Cl]_o - [Cl]_i)/ ([Na]_o - \exp(E_{rev}/25.34)\cdot[Na]_i) \quad (3)$$

Using a linear least squares fitting routine, this equation was fitted to the data in Fig. 5 with a P_{Na}/P_{Cl} value of 0.034 (Fig. 5, unbroken line). A dashed line representing $P_{Na}/P_{Cl} = 0$ is shown for comparison. This indicated that the calcium-activated conductance was indeed predominantly selective for chloride ions, although a small permeability to Na^+ or Ca^{2+} cannot be ruled out.

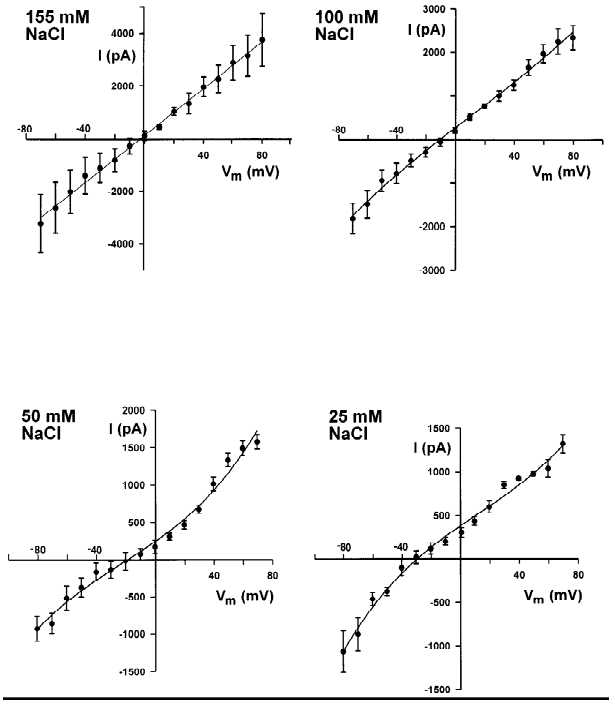

Fig. 4. Averaged *I-V* relationships in patches exposed to different concentrations of intracellular NaCl as indicated. Currents were measured at 0.2 mM calcium and background leakage has been subtracted. Each curve represents the mean of 4 patches. Note that the reversal potential becomes increasingly negative as the NaCl concentration is reduced.

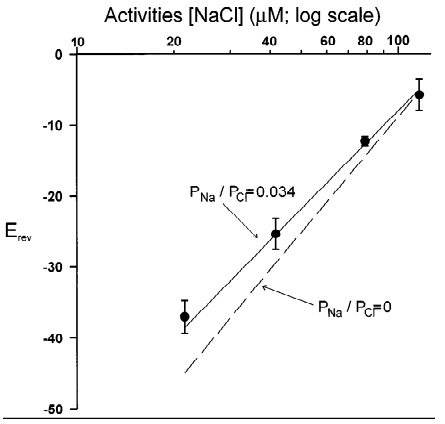

Fig. 5. The chloride selectivity of the calcium-activated currents. The reversal potential (E_{rev}) is plotted against the activity of NaCl (extrapolated from tables in Robinson and Stokes, 1965). The unbroken line shows the experimental reversal potentials fitted with a P_{Na}/P_{Cl} of 0.034. The broken line is the line of best fit when P_{Na}/P_{Cl} is zero. Lines of best fit were calculated using the Goldman-Hodgkin-Katz equation (Eq. 2).

Permeation by Halide Anions

To determine the ionic selectivity of the calcium-activated chloride channel, experiments were performed in which the NaCl in the solution bathing the intracellular (exposed) patch surface was completely replaced by the appropriate sodium salt for these bi-ionic solutions to be at the same concentration as the NaCl in the pipette. Thus the Cl^- was completely replaced by either 140 mM F^-, I^- or Br^-. In each experiment, the 155 mM NaCl solution was applied prior to each test anion application, so that relative conductances could be measured. The solutions were applied to each patch in the following order (numbers represent concentrations in mM):

0 Ca/155 NaCl + 0.2 Ca/140 NaF/140 NaF+ 0.2 Ca/140 NaF/155 NaCl + 0.2 Ca/0 Ca
0 Ca/155 NaCl + 0.2 Ca/140 NaI/140 NaI+ 0.2 Ca/140 NaI/155 NaCl + 0.2 Ca/0 Ca
0 Ca/155 NaCl + 0.2 Ca/140 NaBr/140 NaBr+ 0.2 Ca/140 NaBr/155 NaCl + 0.2 Ca/0 Ca

Figure 6 shows examples of currents recorded from one patch for each of these experimental conditions. It is apparent that the substitution of Cl^- ions by F^-, I^- and Br^- results in a dramatic reduction in the magnitude of

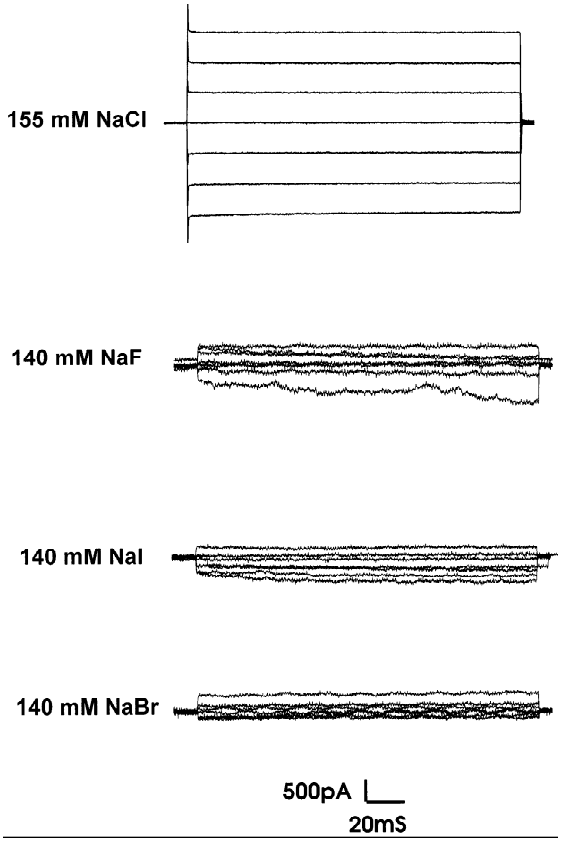

Fig. 6. Calcium-activated chloride currents recorded in a single patch in the presence of chloride, fluoride, bromide and iodide, respectively, at the intracellular membrane surface. The extracellular patch surface was exposed to 140 mM Cl^- solution in all experiments. Currents were elicited by the application of 0.2 mM calcium and background leakage currents have been subtracted. The scale bar applies to all displayed traces.

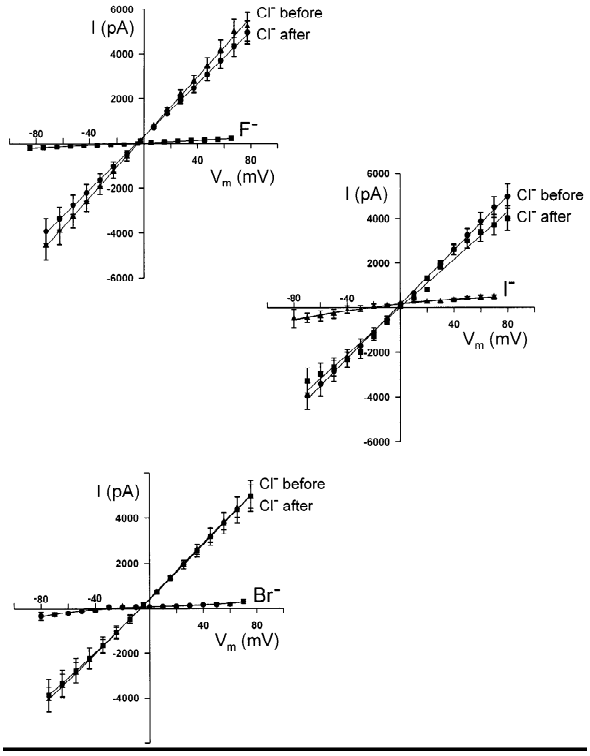

Fig. 7. *I-V* relationships for the halide anions averaged from currents recorded in 5 patches. In each panel, the current response to Cl^- is shown both before and after the application of the test anion. Currents were elicited by the application of 0.2 mM calcium and background leakage currents have been subtracted.

the current. Although the anions were substituted only on the intracellular membrane surface, both inward and outward currents were drastically reduced. Current-voltage relationships averaged from 5 patches are shown in Fig. 7. The *I-V* relationship for each halide anion has been shown together with the *I-V* relationship for Cl^- ions applied before and after each anion.

Accompanying the dramatic decrease in current magnitude, the reversal potentials in the presence of the substituted anions were shifted to more negative potentials. The smallest reversal potential shift was observed with F^- and the largest was observed with Br^-. The following simplification of the Goldman-Hodgkin-Katz equation was used to estimate the relative permeabilities of each test anion relative to chloride:

$$E_{rev} = (RT/zF) \ln \{P_A[A]_o/P_B[B]_i\} \quad (4)$$

where z is the valency of the ions, P_A and P_B are the permeabilities of the anions on the outside and inside membrane surfaces, respectively, and $[A]_o$ and $[B]_i$ are the concentrations of ion A on the outside and B on the inside, respectively. Expressing P_A/P_B in terms of E_{rev} we obtain:

$$P_A/P_B = \exp \{(E_{rev}/-25.34)\cdot([B]_i/[A]_o)\} \quad (5)$$

After substitution of the experimentally derived reversal potentials and concentrations of both anions, P_A/P_B (with A representing Cl^- and B the substituted ion) was determined using this equation. This procedure was followed for both the substituted halide anions and the inorganic anions (*see below*). The relative permeability sequence for halide anions was $Cl^- > F^- > I^- > Br^-$, with the permeability ratios relative to chloride of 1 : 0.73 : 0.41 : 0.25. Values of permeability ratios relative to chloride are plotted against the ionic diameter in Fig. 10.

Permeation by Organic Anions

In an attempt to estimate the minimum pore diameter of the channel, organic anions were substituted in place of chloride. The anions used in these experiments were thiocyanate (SCN^-), acetate$^-$ and gluconate$^-$. The protocol for the application of the control and anion-substituted solutions was similar to that described in the previous section for the halide anions. Examples of current traces recorded in one patch that was sequentially exposed to the Cl^-, SCN^-, acetate$^-$ and gluconate$^-$ are shown in Fig. 8. Leakage currents recorded in the absence of calcium have been subtracted from the displayed responses. Similar results were obtained in each of 5 patches.

It is apparent that all substituted organic anions caused a strong reduction in the calcium-activated current at both positive and negative membrane potentials. The SCN^- caused the least reduction in current, indicating that it was the most permeant of this series of anions. The *I-V* relationships for each organic anion relative to Cl^- were averaged from 5 patches and are shown in Fig. 9. Averaged reversal potentials were then used to calculate the relative permeability of each organic anion relative to chloride. The permeability sequence thus derived was: $Cl^- > SCN^-$ > acetate$^-$ > gluconate$^-$, with permeability ratios relative to Cl^- of 1 : 0.76 : 0.44 : 0.31. On the other hand, the conductivity sequence measured at +50 mV was: $Cl^- > SCN^-$ > gluconate$^-$ > acetate$^-$. Thus, all tested organic anions were appreciably permeant, indicating a minimum pore diameter of >5.8 Å. The permeability ratios of each organic anion relative to chloride have been plotted against their respective molecular diameters in Fig. 10.

Discussion

Comparison with the Frog Calcium-Activated Chloride Channel

Calcium-activated chloride channels were originally identified in olfactory receptor neurons of the frog by

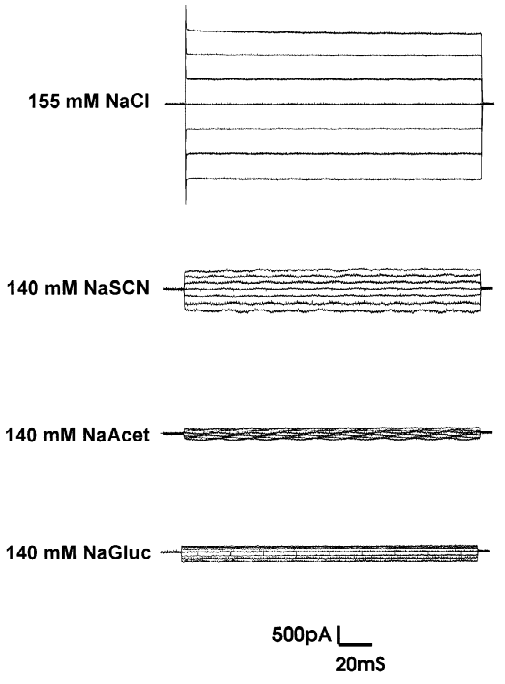

Fig. 8. Calcium-activated chloride currents recorded in a single patch in the presence of chloride, SCN^-, $acetate^-$ and $gluconate^-$, respectively, at the intracellular membrane surface. The extracellular patch surface was exposed to 140 mM Cl^- solution in all experiments. Currents were elicited by the application of 0.2 mM calcium and background leakage currents have been subtracted. The scale bar applies to all displayed traces.

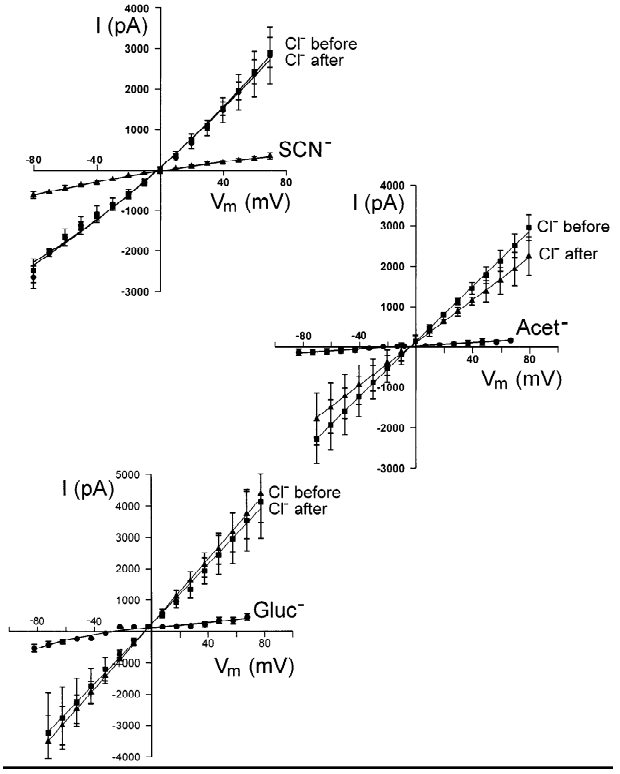

Fig. 9. *I-V* relationships for the organic anions averaged from currents recorded in 5 patches. In each panel, the current response to chloride is shown both before and after the application of the test anion. Currents were elicited by the application of 0.2 mM calcium and background leakage currents have been subtracted.

Kleene and Gesteland (1991) and their presence in olfactory receptor neurons of the rat was confirmed by Lowe and Gold (1993). Lowe and Gold provided evidence for a physiological role for these channels in amplifying the small odorant-induced currents carried by calcium ions through CNG cation channels. There have, however, been no detailed investigations into the biophysical properties of the olfactory calcium-activated chloride channels in any species. In this paper, we have confirmed the presence of a Ca^{2+}-activated Cl^- conductance in dendritic knob membranes of rat olfactory receptor neurons and have characterised some of its biophysical properties.

The calcium concentration required for half-maximal activation of the chloride current is about 26 μM, and there is significant activation of the current at a calcium concentration below 10 μM (Fig. 3*B*). Since the calcium concentration in olfactory receptor neurons increases to micromolar levels during odorant stimulant (Schild et al., 1995; Kashiwayanagi, 1996), the calcium sensitivity of these chloride channels lies within the range expected for them to contribute to the olfactory transduction process.

The properties of the rat and frog olfactory calcium-activated chloride channels are different in several significant respects. The calcium EC_{50} for the rat channel is an order of magnitude higher than it is in the frog. Another significant difference is that the *I-V* relationship of the frog calcium-activated chloride channel displays strong inward rectification, whereas the rat channel displays a linear *I-V* relationship between −80 and +70 mV. It also appears that the density of calcium-activated chloride channels in the dendritic knob of the rat olfactory receptor neuron is at least an order of magnitude higher than in the cilia of the frog. We found that maximum calcium-activated conductances ranged between 30–75 nS in patches for the dendritic knob of rat olfactory receptor neurons, whereas entire cilia of the frog exhibited a maximum magnitude of only 1.3–7.9 nS. it is unlikely that these differences can be explained by differences in recording configurations as our pipettes were sharp (10–15 MΩ) and hence the membrane area of excised patches is likely to have been significantly smaller than the entire membrane area of the space-clamped region of a frog olfactory cilium. Indeed, using noise analysis, Larsson, Kleene and Lecar (1997) have estimated a single channel conductance of 0.8 pS and channel density of about 70 channels $\cdot \mu m^{-2}$ to give a conductance per unit area of about 60 pS $\cdot \mu m^{-2}$. Allowing for a tip diameter in our measurements of about 0.2 μm and a hemispherical

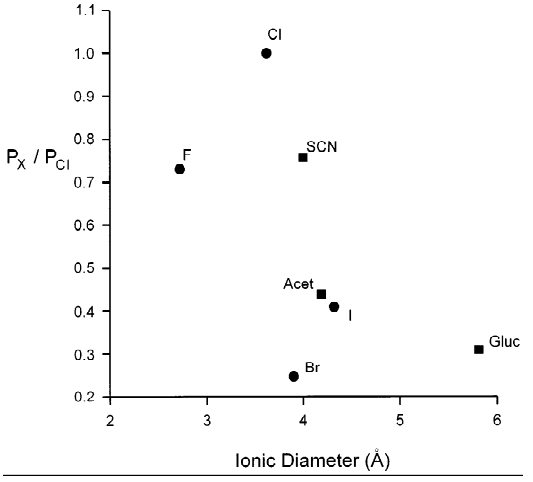

Fig. 10. Plot of the relative permeabilities of all anions tested in this study against their ionic diameters in Å. The filled circles represent the inorganic halide anions and the filled squares represent the organic anions. Since all tested anions were appreciably permeant, the minimum pore diameter must have been at least 5.8 Å.

patch of area of about 0.06 μm^2, our conductance per unit area is in the range from 500 to 1250 $nS \cdot \mu m^{-2}$. One explanation of these differences could be possible effects of the trypsin dissociation in our experiments, with the suggestion that somehow trypsin has altered the properties of the channel itself and maybe also caused a redistribution of channels from the cilia to the dendritic knob. Although such effects seem unlikely, they cannot be unequivocally ruled out. Alternatively, as would seem to be much more probable, the differences may be real and species dependent. If the latter were to be true, the question would then become whether or not any of these species-dependent differences are important for conferring differences on the respective olfactory transduction mechanisms.

Anionic Selectivity of the Ca^{2+}-activated Cl^- Channel

The halide permeability sequence of the rat olfactory calcium-activated chloride channel was: $Cl^- > F^- > I^- > Br^-$. The sequence of unhydrated ionic diameters for these anions is: $I^- > Br^- > Cl^- > F^-$ and the sequence of hydration energies from highest to lowest is: $F^- > Cl^- > Br^- > I^-$. Theoretically, ions with smaller radii are preferred when ion-channel interactions are stronger than ion-water interactions. In these channels it was found that the anions with the larger hydration energies (Cl^- and F^-) were more permeant than those with the lower hydration energies (I^- and Br^-). Since the hydration energy sequence parallels the permeation one for these Ca^{2+}-activated Cl^- channels, it may be concluded that the pore selectivity contains high field strength binding sites. The permeation sequence determined in this study corresponds most closely to sequence 6 of Wright and Diamond (1977). Their sequence 6 (i.e., $Cl^- > F^- > Br^- > I^-$) is characteristic of channels containing high field strength binding sites. In fact, since I^- is more permeable than Br^- in the rat olfactory calcium-activated chloride channel, its binding site has an even higher field strength than predicted by sequence 6.

Pore Diameter of the Ca^{2+} activated Cl^- Channels

We used the organic anions SCN^-, acetate$^-$ and gluconate$^-$ to probe the apparent maximum pore diameter of the Ca^{2+}-activated Cl^- channel. The empirically determined permeation sequence for these organic anions was: $Cl^- > SCN^-$ > acetate$^-$ > gluconate$^-$. Since the ionic diameters for these anions are (in Å), Cl^-: 3.6, SCN^-: 4.0, acetate$^-$: 4.2, and gluconate$^-$: 5.8, the permeation sequence was inversely proportional to the size of the anion. Since gluconate$^-$ was readily permeant, the pore diameter must be at least 5.8 Å. The observed permeability sequence is similar to that described for Cl^- channels in the apical membranes of airway epithelia, except that Cl^- was more permeant than SCN^- (Li, McCann, & Welsh 1990). In Cl^- channels of basolateral membranes of airway epithelia, the permeability sequence of organic anions was exactly the same as that obtained in this study (Li et al., 1990). GABA- and glycine-gated Cl^- channels exhibit a similar permeability sequence to that obtained in this study, except that SCN^- was 4 times more permeable than Cl^- (Fatima-Shad & Barry, 1993).

We would like to acknowledge the help of Mr. Terry Flynn of the Centre for Chemical Analysis of the University of New South Wales, who measured the calcium contamination of some of our solutions by inductively coupled plasma atomic emission spectrometry. In addition, we would like to acknowledge the support of the Australian Research Council.

References

Barry, P.H. 1994. JPCalc, a software package for calculating liquid junction potential corrections in patch-clamp, intracellular, epithelial and bilayer measurements and for correcting junction potential measurements. *J. Neurosci. Methods* **51:**107–116

Dionne, V.E., Dubin, A.E. 1994. Transduction diversity in olfaction. *J. Exp. Biol.* **194:**1–21

Fatima-Shad, K., Barry P.H. 1993. Anion permeation in GABA- and glycine-gated channels of mammalian cultured hippocampal neurons. *Proc. R. Soc. Lond. Ser. B.* **253:**69–75.

Firestein, S., Darrow, B., Shepherd, G.M. 1991. Activation of the sensory current in salamander olfactory receptor neurons depends on a G protein-mediated cAMP second messenger system. *Neuron* **6:**825–835

Frings, S., Seifert, R., Godde, M., Kaupp, U.B. 1995. Profoundly different calcium permeation and blockage determine the function of distinct cyclic nucleotide-gated channels. *Neuron* **15:**169–179

Hamill, O.P., Marty, A., Neher, E., Sakmann, B., Sigworth, F.J. 1981. Improved patch-clamp techniques for high-resolution current recording from cells and cell-free membrane patches. *Pfluegers Arch.* **391:**85–100

Kashiwayanagi, M. 1996. Dialysis of inositol 1,4,5-triphosphate induces inward currents and Ca^{2+} uptake in frog olfactory receptor cells. *Biochem. Biophys. Res. Comm.* **225:**666–671

Kleene, S.J. 1993. Origin of the chloride current in olfactory transduction. *Neuron* **11:**123–132

Kleene, S.J., Gesteland, R.C. 1991. Calcium-activated chloride conductance in frog olfactory cilia. *J. Neurosci.* **11:**3624–3629

Kurahashi, T., Yau, K-W. 1993. Co-existence of cationic and chloride components in odorant-induced current of vertebrate olfactory cells. *Nature* **363:**71–74

Kurahashi, T., Yau, K-W. 1994. Olfactory transduction. Tale of an unusual chloride current. *Current Biology* **4:**256–258

Larsson, H.P., Kleene, S.J., Lecar, H. 1997. Noise analysis of ion channels in non-space-clamped cables: estimates of channel parameters in olfactory cilia. *Biophys. J.* **72:**1193–1203

Li, M., McCann, J.D., Welsh, M.J. 1990. Apical membrane Cl^- channels in airway epithelia: anion selectivity and effect of an inhibitor. *Am. J. Physiol.* **259:**C295–C301

Lowe, G., Gold, G.H. 1993. Nonlinear amplification by calcium-dependent chloride channels in olfactory receptor cells. *Nature* **366:**283–286

Lynch, J.W., Barry, P.H. 1991. Properties of transient K^+ currents and underlying single K^+ channels in rat olfactory receptor neurons. *J. Gen. Physiol.* **97:**1043–1072

Reed, R.R. 1992. Signalling pathways in odorant detection. *Neuron* **8:**205–209

Robinson, R.A., Stokes, R.H. 1965. Electrolyte Solutions. (2nd ed., revised) Butterworths, London

Schild, D., Lischka, F.W., Restrepo, D. 1995. $InsP_3$ causes an increase in apical $[Ca^{2+}]_i$ by activating two distinct current components in vertebrate olfactory receptor cells. *J. Neurophysiol.* **73:**862–866

Wright, E.M., Diamond, J.M. 1977. Anion selectivity in biological systems. *Physiol. Rev.* **57:**109–156